Available online at www.sciencedirect.com
SCIENCE DIRECT®
Journal of Structural Biology 147 (2004) 12–18
Journal of Structural Biology
www.elsevier.com/locate/yjsbi

Similar diffusibility of membrane proteins across the axon–soma and dendrite–soma boundaries revealed by a novel FRAP technique

Takashi Fukano, Hiroshi Hama, and Atsushi Miyawaki*

Laboratory for Cell Function Dynamics, Advanced Technology Development Group, Brain Science Institute, RIKEN 2-1 Hirosawa, Wako-city, Saitama 351-0198, Japan

Received 29 July 2003, and in revised form 17 October 2003

Abstract

In polarized mature neurons, the asymmetrical distribution of proteins between axonal and somatodendritic plasma membrane (PM) domains may be maintained by a diffusion barrier at the axon–soma boundary. At the boundary, a complex containing membrane-associated and cytoskeletal proteins is formed, anchoring axonal membrane proteins and indirectly hindering the diffusion of other membrane proteins. We examined the latter case, i.e., secondary diffusion impedance by comparing the mobility of fluorescently labeled membrane proteins within the axon–soma and dendrite–soma boundaries. We performed fluorescence recovery after photobleaching (FRAP) experiments using mature cultured hippocampal neurons that had been labeled specifically at their PMs with fluorescent proteins (FPs). The maturation of these neurons was confirmed by immunolocalization with Ankyrin-G, which is thought to participate in the creation of the diffusion barrier at the axon–soma boundary. We developed a wide-field microscope equipped with a device (digital micromirror device) composed of 1024×768 binary mirrors at the field-stop, allowing free control of the illumination area and intensity. After the FPs in peripheral processes were photobleached, nonbleached FPs diffused into all the processes at equivalent speeds. These results indicate that the secondary diffusion barrier to exogenously overexpressed membrane proteins is not specific to the axon–soma boundary.

Keywords: Soma; Axon; Dendrite; Fluorescent protein; Fluorescence recovery after photobleaching; Digital micromirror device

1. Introduction

Kobayashi et al. (1992) first reported the presence of a diffusion barrier at the axonal hillock with fluorescently labeled phospholipids. In contrast, Winckler and Poo (1996) observed free diffusion of the artificial lipid DiI across the axon hillock following labeling of a dendrite or distal portion of an axon. In these two studies, which analyzed bulk flow of lipids, it was difficult to confirm specific incorporation of the lipid dye into the plasma membrane. Later, Winckler and his colleagues (1999) examined the diffusion of membrane proteins, by a direct approach to elucidate their asymmetrical distribution in neurons. Following the manual movement of membrane proteins along the axon using optical tweezers, they detected high impedance of diffusion in the initial segment of the axon, 20–90 μm from the soma. They proposed that a tethering interaction between membrane proteins and cytoskeleton underlies the diffusion impedance. The impedance was also observed both for Thy-1, linked only to lipids in the outer membrane leaflet, and for other membrane glycoproteins that bind the lectin ConA. Therefore, the sheer density of membrane proteins retained in the initial segment creates a physical impediment to axonal diffusion of peripheral proteins such as Thy-1. Quite recently, Nakata et al. (2003) followed the dynamics of individual phospholipid molecules in developing hippocampal neurons to demonstrate formation of the diffusion barrier in the PM at the axon–soma boundary. They found

* Corresponding author. Fax: +81-48-467-5924.
E-mail address: matsushi@brain.riken.go.jp (A. Miyawaki).

1047-8477/$ - see front matter © 2003 Elsevier Inc. All rights reserved.
doi:10.1016/j.jsb.2003.11.002

that lipid mobility was reduced at the initial segment, which correlated with the expression of a cytoskelton protein, ankyrin, and with the maturity of the cultured neurons.

Assuming that multiple membrane proteins shuttle between the soma and processes, it will be interesting to determine if their movement is impeded specifically at the axon–soma boundary. To examine the existence of such a traffic jam, we measured the diffusability of GFP-fusion membrane proteins from the soma to either dendrites or axons in mature neurons. For the global observation, we carried out fluorescence recovery after photobleaching (FRAP) experiments using an wide-field fluorescence microscope system equipped with a computer-controlled digital micromirror device (Fukano and Miyawaki, 2003; Hanley et al., 1999; Liang et al., 1997; MacAulay and Dlugan, 1998).

2. Materials and methods

2.1. Materials

The cDNA of Thy-1 was a gift from Dr. G. Kondo at Osaka University. The plasmid DNA for GluR2-GFP was from Dr. Y. Hayashi at RIKEN/MIT. Interference filters were from Omega Optical.

2.2. Gene construction

Lyn-Venus was created by extending Venus cDNA at the 5′ end with a sequence encoding the 22 N-terminal amino acids of the nonreceptor tyrosine kinase, Lyn (Sawano et al., 2002). Venus-ER was obtained by extending Venus cDNA at the 5′ end with the sequence encoding the signal peptide from calreticulin and at the 3′ end with the sequence encoding the ER retention signal (KDEL) (Miyawaki et al., 1997). The sequence for rat neuromodulin was fused to DsRed gene (Clontech) to create the cDNA for DsRed-PM. These cDNAs were subcloned into pIND (Invitrogen).

2.3. Cell culture

Dissociated hippocampal neurons were prepared from Wistar rat embryos (embryonic days 17–18) by digestion with papain (Wako Chemical)/DNase I (Takara) as described (Kossel et al., 1997). Cells were plated onto poly-L-lysine (Sigma) coated glass coverslips (plating density was 20 000 cells/cm^2). Cultured cells were kept at 37 °C in 5% CO_2. They were maintained for about 1 month by two-step medium treatment as follows: MEM containing N2-supplement (Gibco-BRL) and 20% FBS for the first 4 h, and subsequently changed to MEM containing N2-supplement and 2% FBS. Glial cells were not eliminated.

2.4. Transfection

Hippocampal neurons were transfected following a calcium phosphate transfection protocol described as previously (Xia et al., 1996).

2.5. Immunostaining

Cultured cells were fixed with 4% paraformaldehyde/100 mM sodium phosphate buffer (pH 7.2) for 20 min at room temperature and permealized with 0.05% Triton X-100/PBS (phosphate-buffered saline) for 90 s at room temperature. After blocking with 5% bovine serum albumin, cells were reacted with anti-Ankyrin-G mouse monoclonal antibody (Ab) (Santa Cruz, 1:200), and with Alexa-546-conjugated goat anti-mouse IgG Ab (Molecular Probes, 1:500). The fluorescence was observed by Olympus FV500 confocal microscope.

2.6. FRAP experiments

Excitation power was reduced to 5–10% using the DMD-based modulation to image cell samples. Images (exposure time, 200–500 ms) were collected at 3 s intervals. The selected regions containing the processes were photobleached at 100% excitation power. After background subtraction, the fluorescence intensity has been normalized to the initial value and plotted. The final fluorescence intensities did not reach the initial values. The difference between the initial and final values is usually referred to as the ''immobile fraction'' in FRAP analyses. This is not the case, however, in our experiments. Because DMD exhibits a relatively poor extinction factor, the cell soma was not protected completely from the bleaching light. Therefore, the immobile fraction was measured by comparing the ratio of fluorescence intensities in the soma and photobleached processes before photobleaching and after recovery (Cole et al., 1996). The recovery time constants were calculated by least-squares regression of the equation, $I(t) = A[1 - \exp(-t/\tau)]$, where τ is the time constant, A is the mobile fraction, and $I(t)$ is the fluorescence intensity. Phase-contrast images of cells were taken before and immediately after FRAP analyses to ensure that there were no significant changes in cell shape and position.

3. Results and discussion

3.1. A wide-field microscope equipped with a digital micromirror device

We modified a conventional epi-fluorescence microscope (IX70, Olympus) by placing a digital micromirror device (DMD) removed from a commercial DLP (digital

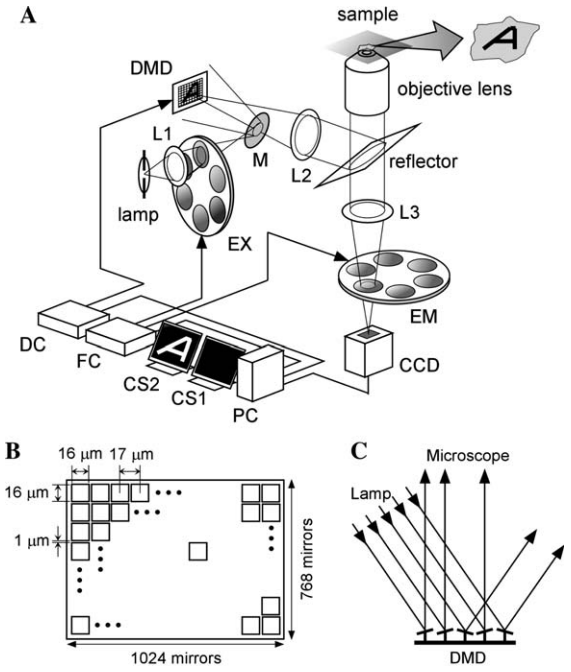

Fig. 1. Wide-filed fluorescence microscope with digital micromirror device. (A) Schematic of the DMD microscope. The DMD (Texas Instruments, TX), a filter exchanger controller (Lambda 10-2, Sutter Instruments, Novato, CA), and a cooled CCD camera (ORCA-ER, Hamamatsu Photonics, Hamamatsu) were controlled using MetaFluor 4.6 software (Universal Imaging, Media, PA), modified in-house to facilitate the designing of illumination patterns on the fluorescence micrograph displayed on the computer screen. L1, collector lens; L2, collimater lens; L3, tube lens; EX, excitation filter wheel; EM, emission filter wheel; PC, personal computer; CS1, CS2, computer screen; FC, filter controller; and DC, DMD controller. (B) Pixel layout on the DMD chip. (C) Binary operation of micromirrors.

light processing) projector (U3-1080, PLUS) in the plane of the field iris in the excitation path (schematic diagram, Fig. 1A). The DMD chip is composed of 1024×768 micromirrors; each size is $16\,\mu m \times 16\,\mu m$, the inter-mirror gap is $1\,\mu m$, so the pixel pitch is $17\,\mu m$ (Fig. 1B). The effective reflectance for visible light is about 70%, which principally depends on the fill factor and the transmittance of protection windows of the DMD. As each micromirror could be electronically set to tilt by $\pm 10°$ with respect to the DMD surface, the device acts as a reflection-type spatial light modulator (Fukano and Miyawaki, 2003; Hanley et al., 1999; Liang et al., 1997; MacAulay and Dlugan, 1998) (Fig. 1C). When the micromirrors are set at $+10°$, excitation light originating from a lamp and filtered by an excitation filter (EX) is directed to the microscope. On the other hand, when they are set at $-10°$, light is deflected outside the microscope. A bi-convex lens (L1) and a mirror (M) were positioned such that a diverging cone of rays arrives at the DMD chip. This configuration reduced the diffraction pattern arising from the DMD chip lattice. Bleaching and image acquisition were coordinated by PC software designed to edit bleaching regions on the acquired fluorescence images. As the mirrors fluctuate between the on and off positions at approximately 1 kHz, the intensity of illumination can be reduced variably by changing the time ratio of on to off.

To bleach samples, the light from a mercury lamp was passed through a 420 nm long-pass filter and maximally reflected onto the DMD chip. Although laser scanning confocal microscopy with acousto-optical tunable filters (AOTFs) allows bleaching and image acquisition within any drawn regions of interest, laser use limits the possible excitation wavelengths, and requires special instrumentation and expertise. In particular, the use of xenon or mercury lamps would allow the bleaching of DsRed (Clontech), a widely used red FP. Due to the lower degree of photosensitivity of this protein (Baird et al., 2000), the laser providing the excitation wavelength for this FP (green He/Ne (543 nm)) is too weak, although there are strong green lasers available, such as Nd:YAG (532 nm) and Ar/Kr (568 nm).

3.2. Mature cultured neurons labeled specifically at the plasma membranes with fluorescent proteins

Following 10 days in culture (DIV 10), rat hippocampal neurons were examined for proper differentiation of the axonal and somatodendritic domains using an antibody against Ankyrin-G, the axonal protein proposed to participate in the creation of the diffusion barrier in the initial segment. Ankyrin-G was found to be localized exclusively throughout the axonal initial segment, confirming the maturation of the neurons (Fig. 2A). Such axon-specific immunolabeling for Ankyrin-G was observed in all DIV 10 neurons examined. While hippocampal neuron maturation is assumed to remain incomplete after 10 days in culture (Craig and Banker, 1994), the neurons in the present study matured very quickly, possibly due to the high density of culture and presence of glial cells (Kossel et al., 1997). To employ FRAP, we used a lipid-modified intracellular chimeric protein expected to be affected by the traffic jam. A bright variant of *Aequorea* GFP, Venus (Nagai et al., 2002), was fused to the 22 amino acid N-terminus of the nonreceptor tyrosine kinase, Lyn (Lyn-Venus). This chimeric protein is anchored to the plasma membrane through palmitate and myristate groups (Resh, 1994). Mature neurons were transfected with cDNA encoding Lyn-Venus. The cDNA was cloned into a tightly regulated, inducible expression vector, pIND (Invitrogen). One to two days after transfection with pIND/Lyn-Venus and pVgRXR (Invitrogen), expression was shut off for 12 h by removing the inducer Ponasterone-A from the medium. This procedure minimized the accumulation of nascent fluorescent chimeric proteins in internal membranes, making PM-specific labeling possible. Fig. 2B shows a fluorescence

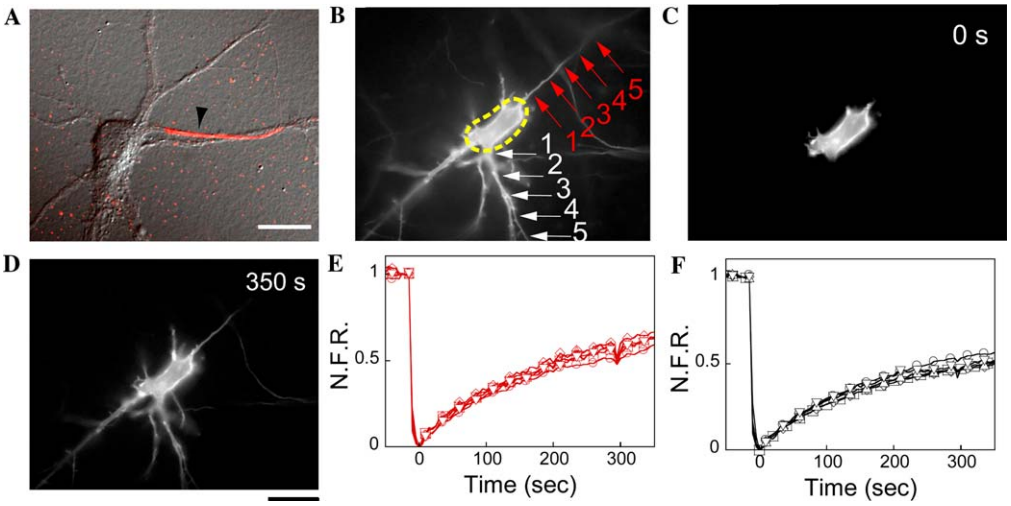

Fig. 2. Diffusion of Lyn-Venus from the soma into the processes of DIV 10 neurons. (A) Indirect immunofluorescence of a rat hippocampal neuron with anti-Ankyrin-G antibody showing the localization of the protein in the initial segment of an axon (indicated by a black arrowhead). Scale bar, 20 μm. (B) Fluorescence micrograph of a rat hippocampal neuron expressing Lyn-Venus. The bleached region covering the processes is bounded by a yellow dotted line. Segments were made every 10 μm along the axon and one of the dendrites, indicated by red and white arrows, respectively. (C) Venus visualization after a 10-s bleaching. (D) Fluorescence image following a 350-s recovery period. Scale bar, 20 μm. (E and F) Time courses of fluorescence recovery at the segments defined in (B) on the axon and dendrite, respectively. The fluorescence signals from segments 1–5 were normalized to the initial values that were corrected for the amount of fluorescence removed during photobleaching (N.F.R: normalized fluorescence recovery). Data points at 15-s intervals are shown using open circles, squares, up-triangles, down-triangles, and diamonds, respectively. Because DMD exhibits a relatively poor extinction factor, probably due to diffraction, the cell somata were not completely protected from the bleaching light. Therefore, the sum total of the fluorescence over the neuron decreased to various levels. Fluorescence images were captured using an excitation filter (475DF40), an emission filter (535AF45), and a dichroic mirror (505DRLPXR). The dichroic mirror also allowed the intense light passing through the UV-cut filter to reach the sample. Thus, the wavelength of the bleaching light was limited to between 420 and 505 nm. Primary neurons were prepared from Wistar rat embryos (E17-18) as described previously (Kossel et al., 1997). Cultured neurons were grown on a 35-mm glass-bottomed dish in chemically defined medium containing N2-supplement (Gibco-BRL) and 2% FBS.

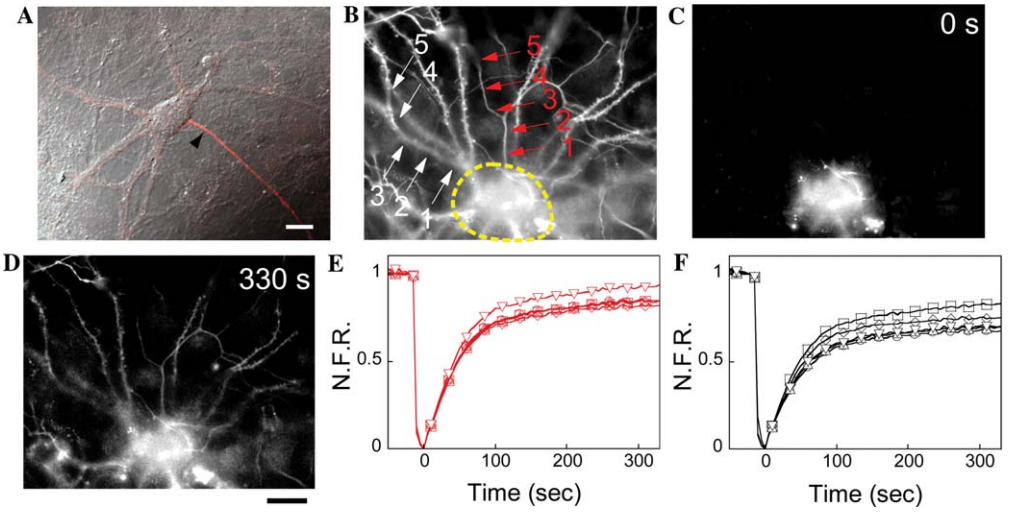

Fig. 3. Diffusion of Lyn-Venus from the soma into the processes of DIV 21 neurons. (A) Indirect immunofluorescence of an old neuron with anti-Ankyrin-G antibody. The axon is indicated by a black arrowhead. Scale bar, 20 μm. (B) Fluorescence micrograph of a neuron expressing Lyn-Venus, as shown in Fig. 2B. Segments were made as in Fig. 2B. (C) Venus visualization after a 10-s bleaching. (D) Fluorescence image following a 330-s recovery period. Scale bar, 20 μm. (E and F) Time course of fluorescence recovery at the segments defined in (B) on the axon and dendrite, respectively. The fluorescence signals from segments 1–5 are plotted as in Figs. 2E and F.

micrograph of a mature neuron exhibiting controlled expression of Lyn-Venus. Confocal laser scanning microscopy confirmed selective labeling of the PM in all experiments. The axon (red arrows), identified morphologically, was verified also by immunohistochemical staining for tau (data not shown).

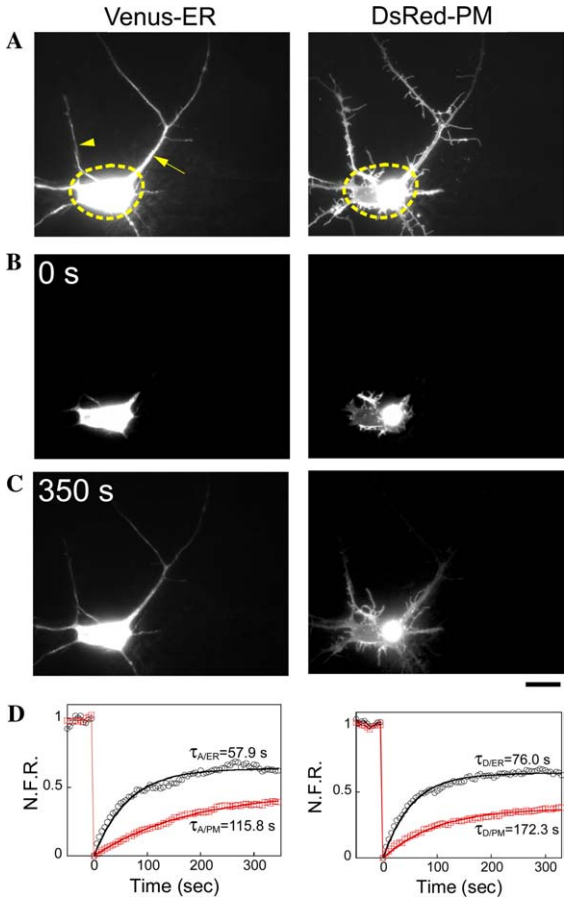

Fig. 4. Diffusion of Venus-ER and DsRed-PM from the soma to processes. (A) Fluorescence micrographs of a rat hippocampal neuron containing Venus (left) and DsRed (right) proteins, as shown in Fig. 2B. (B) Fluorescence images for Venus (left) and DsRed (right) after a 10-s bleaching. (C) Images obtained after a 350-s recovery. Scale bar, 20 μm. (D) Left: Time course of fluorescence recovery of the red fluorescence at the PM (red squares) and the yellow fluorescence in the ER (black circles) at the point indicated by the arrow (A) on the axon. Right: Time course of recovery of the red fluorescence at the PM (red squares) and the yellow fluorescence in the ER (black circles) at the point indicated by the arrowhead (A) on the dendrite. An intense light >420 nm was reflected by a mirror in a filter cube for bleaching. Yellow (Venus) and red (DsRed) fluorescence images were captured sequentially every 5 s. The glass reflector with 4% reflection and 96% transmission was placed in the filter cube (Sawano et al., 2002). The excitation and emission filters were placed in the filter wheels in the excitation and emission paths, respectively. Venus fluorescence was detected using 475DF40 and 535AF45 (Omega); DsRed fluorescence was detected using 550DF30 and 575ALP (Omega).

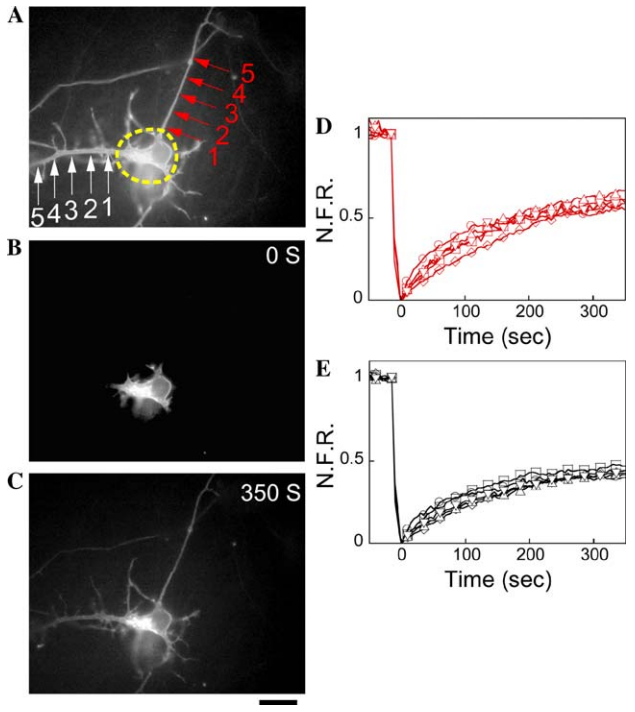

Fig. 5. Diffusion of Thy1-EGFP from the soma into the processes of DIV 10 neurons. (A) Fluorescence micrograph of a rat hippocampal neuron expressing Thy1-EGFP as shown in Fig. 2B. Segments were made as in Fig. 2B. (B) EGFP visualization after a 10-s bleaching. (C) Fluorescence image following a 350-s recovery period. Scale bar, 20 μm. (D and E) Time course of fluorescence recovery at the segments defined in (A) on the axon and dendrite, respectively. The fluorescence signals from segments 1–5 are plotted as in Figs. 2E and F.

3.3. Measurements of the diffusability of fluorescently labeled membrane proteins from the soma to either dendrites or axons

Using the illuminator containing the DMD, we exposed a region (outside of the region bounded by a yellow dotted line in Fig. 2B) to intense light (>420 nm) to bleach. The cell soma was excluded from the bleaching. After 10 s, all the processes were darkened (Fig. 2C). Then, the whole cell was illuminated repeatedly with weak, uniform 470-nm light to acquire a series of images. We did not identify any spontaneous recovery of fluorescence, such as triplet-state recovery (Verkman, 1999) and photochromism (Dickson et al., 1997); when cultured neurons were fixed in paraformaldehyde, the fluorescence recovery in the cellular processes after photobleaching was totally abolished (results not shown). Thus, fluorescence recovery in the processes can be ascribed to the movement of unbleached Venus-containing proteins from the soma. After 330 s, both the axon and dendrites became fluorescent to the same extent (Fig. 2D). It should be possible to calculate the diffusion coefficient of the proteins from the fluorescence distribution along the processes at successive times. Under a wide-field microscope, however, the fluorescence intensity depends on the thickness of the object; for example, varicosities and forks of processes give strong fluorescence, making it impossible to obtain accurate fluorescence–distance curves. Thus, we evaluated diffusion semi-quantitatively by calculating fluorescence recovery time constants at multiple points along the neuronal processes. The proximal portion of the axon, corresponding to the initial segment designated by Winckler et al. (1999) was partitioned into

five segments; the time course of fluorescence recovery in each segment was plotted and fitted to a single exponential component curve (Fig. 2E). The fluorescence recovery in the proximal portion of a dendrite (indicated by white arrows in Fig. 2B) was also examined (Fig. 2F). The time constants for fluorescence recovery and immobile fractions should reflect the diffusion impedance of membrane proteins. Six independent experiments gave values of 106 ± 36 s and $37 \pm 21\%$ for axons and 94 ± 26 s and $36 \pm 15\%$ for dendrites (Table 1), indicating that membrane diffusibility is indistinguishable between the two boundaries. Similar results were obtained from FRAP experiments on DIV 10 neurons using wheat germ agglutinin (WGA)-FITC and a GFP/glutamate receptor type 2 fusion protein (GFP-GluR2) (Table 1).

Next, we examined the diffusability of Lyn-Venus through the axonal and dendritic membranes of older neurons (DIV 21). Ankyrin-G was again localized to the axonal initial segment (Fig. 3A). The fluorescence recovered to similar extent with similar time constants in the axons and dendrites (immobile fraction, $17 \pm 9\%$ vs. $10 \pm 9\%$; time constant, 56 ± 16 s vs. 64 ± 16 s, respectively) (Figs. 3B–F and Table 1). Interestingly, Lyn-Venus fluorescence recovered 1.5- to 2.0-fold faster and more efficiently than in DIV 10 neurons, suggesting that the diffusion through the PM across all soma/process boundaries becomes more active as the neurons get old.

As the fluorescence recovery along processes may depend on geometric factors such as process shape and thickness, we compared the diffusibility of labeled proteins through the PM with that through the endoplasmic reticulum (ER). We labeled the PM and ER using different color fluorescent proteins for dual-color FRAP analysis. A red fluorescent protein, DsRed (Clontech), was fused to a membrane-resident anchoring protein, neuromodulin/GAP43. The resulting chimeric protein, DsRed-GAP43, was localized specifically to the PM (DsRed-PM) (Fig. 4A, right). Even at later time points (DIV >20), both DsRed-PM and the endogenous GAP43 only partially localized to the axon (data not shown). Thus, the distribution of DsRed-PM in the somatodendrite domain as well as in the axonal domains does not signify the immaturity of the neuron. On the other hand, Venus was targeted to the ER lumen by the addition of a C-terminus KDEL ER-retention sequence and an upstream calreticulin signal sequence. Assuming continuity of the ER lumen throughout the cell (Subramanian and Meyer, 1997), the mobility of this chimeric protein (Venus-ER) serves as an internal control. Intense light, with a wavelength longer than 420-nm, was effective in bleaching both DsRed and Venus (Fig. 4B). Following bleaching, all processes were re-labeled equally with both yellow and red fluorescence (Fig. 4C). We quantified the time courses (Fig. 4D) of fluorescence recovery at two points in the axon and the dendrite (indicated by an arrow and an arrowhead, respectively, in Fig. 4A). The relative speed of recovery of red to yellow fluorescence was almost the same in the observed axon–soma and dendrite–soma boundaries. A similar differential speed of recovery through the PM and ER was also observed along the other dendrites (data not shown). These results indicate a similar efficiency of diffusion through the PM across all soma/process boundaries.

Interestingly, when Thy-1-EGFP was used, the recovery time increased with the distance from the cell soma (Fig. 5), indicating attenuated mobility of Thy-1 protein along processes. Such distance-dependence of fluorescence recovery was more evident in the axon than dendrite.

3.4. Equal mobility of membrane proteins within the axon–soma and dendrite–soma boundaries

Our present study measured the translational diffusibility of a large number of labeled proteins through the PM across the boundaries of the soma and peripheral processes simultaneously. All the labeled proteins were localized specifically to the PM and showed widespread distribution. We observed slight impedance of the diffusion of Thy-1 at the axon–soma boundary, somewhat supporting previous reports (Nakata et al., 2003; Winckler et al., 1999). It should be noted, however, that our experimental protocol differed; while their studies monitored the behavior of endogenous membrane pro-

Table 1
Fluorescence recovery time constants and the immobile fractions measured in the axons and dendrites

Type	Construct	*N*	Time constant (s)		Immobile fraction (%)	
			Axon	Dendrite	Axon	Dendrite
Membrane-anchoring	Lyn-Venus	6	106 ± 36	94 ± 26	37 ± 21	36 ± 15
		7	56 ± 16[a]	64 ± 16[a]	17 ± 9[a]	10 ± 9[a]
Membrane-anchoring	DsRed-PM	5	131 ± 71	125 ± 64	74 ± 17	68 ± 21
ER-retention	Venus-ER	5	137 ± 39	128 ± 47		
Transmembrane	GFP-GluR2	2	79 ± 10	74 ± 16	23 ± 6	22 ± 4
Lectin	WGA-FITC	5	172 ± 62	146 ± 38	73 ± 8	75 ± 8

[a] Data from DIV 21 neurons.

teins (Winckler et al., 1999) or individual lipid molecules (Nakata et al., 2003), we overexpressed proteins fused to FPs. Therefore, it remains possible that the number of tethering cytoskeletal proteins is limited, resulting in inefficient tethering of exogenously overexpressed membrane proteins. Our data do not deny the existence of the primary diffusion barrier composed of endogenous axonal proteins and the cytoskelton proteins. Our concern was if the primary barrier creates a traffic jam that indirectly impedes diffusion of wide-spreading membrane proteins. What is important here is that the traffic jam was observed equally in both axons and dendrites. These results suggest that a similar complex is formed at the dendrite–soma boundary, although asymmetric distribution of membrane proteins at the dendrite–soma boundary has been less examined. It should be noted, furthermore, that the diffusion impedance was less observed in older neurons. It is therefore possible that the matured axon–soma boundary immobilizes only specific proteins, while improving traffic conditions of other unrelated proteins. Global observation of fluorescent membrane protein movement may provide a valuable means to explore the sorting of membrane proteins from a different perspective.

Acknowledgments

The authors would like to thank Drs. T. Shimizu, Y. Kawano, and Y. Aono for technical support. This work was supported in part by grants from CREST (the Japan Science and Technology Corporation) and through the Special Coordination Fund for the promotion of the Ministry of Education, Culture, Sports, Science and Technology of the Japanese government.

References

Baird, G.S., Zacharias, D.A., Tsien, R.Y., 2000. Biochemistry, mutagenesis, and oligomerization of DsRed, a red fluorescent protein from coral. Proc. Natl. Acad. Sci. USA 97, 11984–11989.

Cole, N.B., Smith, C.L., Sciaky, N., Terasaki, M., Edidin, M., Lippincott-Schwartz, J., 1996. Diffusional mobility of Golgi proteins in membranes of living cells. Science 273, 797–801.

Craig, A.M., Banker, G., 1994. Neuronal polarity. Annu. Rev. Neurosci. 17, 267–310.

Dickson, R.M., Cubitt, A.B., Tsien, R.Y., Moerner, W.E., 1997. On/off blinking and switching behaviour of single molecules of green fluorescent protein. Nature 388, 355–358.

Fukano, T., Miyawaki, A., 2003. Whole-field fluorescence microscope with digital micromirror device: imaging of biological samples. Appl. Opt. 42, 4119–4124.

Hanley, Q.S., Verveer, P.J., Gemkow, M.J., Arndt-Jovin, D., Jovin, T.M., 1999. An optical sectioning programmable array microscope implemented with a digital micromirror device. J. Microsc. 196, 317–331.

Kobayashi, T., Storrie, B., Simons, K., Dotti, C.G., 1992. A functional barrier to movement of lipids in polarized neurons. Nature 359, 647–650.

Kossel, A.H., Williams, C.V., Schweizer, M., Kater, S.B., 1997. Afferent innervation influences the development of dendritic branches and spines via both activity-dependent and non-activity-dependent mechanisms. J. Neurosci. 17, 6314–6324.

Liang, M., Stehr, R.K., Krause, W., 1997. Confocal pattern period in multiple-aperture confocal imaging systems with coherent illumination. Opt. Lett. 22, 751–753.

Miyawaki, A., Llopis, J., Heim, R., McCaffery, J.M., Adams, J.A., Ikura, M., Tsien, R.Y., 1997. Fluorescent indicators for Ca^{2+} based on green fluorescent proteins and calmodulin. Nature 388, 882–887.

MacAulay, C., Dlugan, A., 1998. Use of digital micromirror decices in quantitative microscope. Proc. SPIE 3260, 201–206.

Nagai, T., Ibata, K., Park, E.S., Kubota, M., Mikoshiba, K., Miyawaki, A., 2002. A variant of yellow fluorescent protein with fast and efficient maturation for cell-biological applications. Nat. Biotechnol. 20, 87–90.

Nakata, C., Ritchie, K., Oba, Y., Nakamura, M., Hotta, Y., Iino, R., Kasai, R.S., Yamaguchi, K., Fujiwara, T., Kusumi, A., 2003. Accumulation of anchored proteins forms membrane diffusion barriers during neuronal polarization. Nat. Cell Biol. 5, 626–632.

Resh, M.D., 1994. Myristylation and palmitylation of Src family members: the fats of the matter. Cell 76, 411–413.

Sawano, A., Hama, H., Saito, N., Miyawaki, A., 2002. Multicolor imaging of Ca^{2+} and protein kinase C signals using novel epifluorescence microscopy. Biophys. J. 82, 1076–1085.

Subramanian, K., Meyer, T., 1997. Calcium-induced restructuring of nuclear envelope and endoplasmic reticulum calcium stores. Cell 89, 963–971.

Verkman, A.S., 1999. Green fluorescent protein as a probe to study intracellular solute diffusion. In: Conn, P.M. (Ed.), Methods in Enzymology. Academic Press, New York, pp. 250–264.

Xia, Z., Dudek, H., Miranti, C.K., Greenberg, M.E., 1996. Calcium influx via the NMDA receptor induces immediate early gene transcription bya MAP kinase/ERK-dependent mechanism. J. Neurosci. 16, 5425–5436.

Winckler, B., Poo, M.-m., 1996. No diffusion barrier at axon hillock. Nature 379, 213.

Winckler, B., Forscher, P., Mellman, I., 1999. A diffusion barrier maintains distribution of membrane proteins in polarized neurons. Nature 397, 698–701.